Journal of Hazardous Materials 172 (2009) 928–934

Contents lists available at ScienceDirect

Journal of Hazardous Materials

journal homepage: www.elsevier.com/locate/jhazmat

# Modeling of arsenic adsorption kinetics of synthetic and contaminated groundwater on natural laterite

Abhijit Maiti, Himanshu Sharma, Jayanta Kumar Basu, Sirshendu De*

*Department of Chemical Engineering, Indian Institute of Technology, Kharagpur, Kharagpur, 721302, India*

ARTICLE INFO

*Article history:*
Received 1 March 2009
Received in revised form 20 July 2009
Accepted 20 July 2009
Available online 8 August 2009

*Keywords:*
Arsenic removal
Shrinking core model
Laterite
Pore diffusivity coefficient

ABSTRACT

A simple shrinking core model is applied to predict the adsorption kinetics of arsenite and arsenate species onto natural laterite (NL) in a stirred tank adsorber. The proposed model is a two-resistance model, in which two unknown parameters, external mass transfer coefficient ($K_f$) and pore diffusion coefficient ($D_e$) are estimated by comparing the simulation concentration profile with the experimental data using a nonlinear optimization technique. The model is applied under various operating conditions, e.g., initial arsenic concentration, NL dose, NL particle size, temperature, stirring speed, etc. Estimated values of $D_e$ and $K_f$ are found to be in the range of 2.2–2.6 $\times 10^{-11}$ m$^2$/s and 1.0–1.4 $\times 10^{-6}$ m/s at 305 K for different operating conditions, respectively. $D_e$ and $K_f$ values are found to be increasing with temperature and stirrer speed, respectively. Calculated values of Biot numbers indicate that both external mass transfer and pore diffusion are important during the adsorption. The model is also applied satisfactorily to predict the arsenic adsorption kinetics of arsenic contaminated groundwater–NL system and can be used to scale up.



## 1. Introduction

Arsenic is a toxic pollutant and poses a serious health risk in many countries of the world. India [1], Bangladesh [1,2], USA [3], Chile [4], Mexico [5] and Taiwan [6], have been affected by arsenic contamination, well above the WHO guideline value of 10 μg/l or the prevailing national standards set by respective countries.

Different technologies have been developed to remove arsenic from both water and wastewater. Technologies include the conventional process of oxidation [7] adsorption onto coagulated flocs [8,9], ion exchange [10], membrane techniques [11,12], etc. Various technologies for arsenic removal are described in recent review literature [13,14]. It has been widely recognized that adsorption on adsorbent media removes arsenic effectively from water and wastewater. Different adsorbents like alumina [15–17], hydrous ferric oxide loaded activated carbon [18], iron oxide minerals [19], zero valent iron corrosion [20], synthetic birnessite [21], goethite [22], laterite [23–26], polymer-supported hydrated iron (III) oxide [27], ferrate [28], fly ashes [29], ferrihydrite [30], synthetic zeolites [31], nano-activated alumina [32], iron-doped activated carbon [33], rice polish [34], have been widely studied by various researchers successfully. Although equilibrium capacity and column breakthrough behavior of arsenate and arsenite in various adsorbents are explored thoroughly, the kinetic modeling of arsenite and arsenate within adsorbent particles is scant in literature. The kinetic data obtained from stirred tank adsorber in the laboratory can be used to generate important process parameters like, mass transfer coefficient ($K_f$), pore diffusivity ($D_e$), etc. for various adsorbent/arsenic species systems.

These parameters are further useful for fixed bed modeling and scaling up of the batch adsorber. In order to estimate the parameters for wider operating conditions, mathematical modeling of process kinetics is required. To develop a mathematical model that describes the adsorption dynamics, following informations are required:

(i) The maximum level of adsorption attained in a sorbent/sorbate system as a function of the sorbate liquid phase concentration, i.e., the equilibrium data.
(ii) A mathematical representation of associated rate of adsorption, which is controlled by the two resistances mainly, external mass transfer from bulk solution to adsorbent surface across the boundary layer surrounding the adsorbent particle and intra-particle diffusion within the pore of the adsorbent particles.

The pore diffusion model outlined in this paper is based on the unreacted shrinking core model [35] with pseudo-steady-state approximation. The assumptions made in this model are as follows: (a) pore diffusion is independent of adsorbate concentration; (b) pseudo-steady-state approximation is valid; (c) the driving force

* Corresponding author. Tel.: +91 3222 283926; fax: +91 3222 255303.
*E-mail address:* sde@che.iitkgp.ernet.in (S. De).

0304-3894/$ – see front matter © 2009 Elsevier B.V. All rights reserved.
doi:10.1016/j.jhazmat.2009.07.140

**Nomenclature**

| | |
|---|---|
| Bi | Biot number (dimensionless) |
| $C_t$ | liquid phase concentration at time $t$ (mg/l) |
| $C_{et}$ | equilibrium liquid phase concentration at time $t$ (mg/l) |
| $C_0$ | initial liquid phase concentration (mg/l) |
| $C^*_{t,\text{exp}}$ | experimental value of non-dimensional bulk concentration at time $t$ |
| $C^*_{t,\text{cal}}$ | calculated value of non-dimensional bulk concentration at time $t$ |
| $D_e$ | effective diffusion coefficient in the adsorbent ($m^2/s$) |
| $K_f$ | liquid phase mass transfer coefficient (m/s) |
| $k_0$ | Langmuir isotherm constant (l/mg) |
| $N(t)$ | adsorption rate at time $t$ (mg/s) |
| $pH_{ini}$ | initial pH of solution |
| $R$ | adsorbent particle radius (m) |
| $R_f$ | radius of concentration front (m) |
| $r$ | non-dimensional radius of adsorption front |
| $t$ | time (s or min) |
| $V$ | volume of batch reactor (l) |
| $W$ | mass of adsorbent (g) |
| $Y_e$ | solid phase concentration at equilibrium (mg/g) |
| $Y_{et}$ | solid phase concentration at time $t$ (mg/g) |
| $Y_s$ | Langmuir isotherm constant (l/g) |
| $\bar{Y}_t$ | average solid phase concentration at time $t$ (mg/g) |

*Greek symbols*

| | |
|---|---|
| $\rho$ | adsorbent density ($kg/m^3$) |

*Subscripts*

| | |
|---|---|
| $f$ | liquid phase |
| 0 | initial |
| $t$ | at time $t$ |

*Superscript*

| | |
|---|---|
| * | non-dimensional |

of the mass transfer in the film is linear; (d) adsorbent particles are spherical and adsorption sites are uniformly distributed.

The above model is used to describe the kinetics of arsenite and arsenate adsorption on natural laterite (NL). Values of effective pore diffusivity ($D_e$) and mass transfer coefficient ($K_f$) are evaluated for arsenic–NL system using an optimization technique.

## 2. Theory

It is found in the earlier works that adsorption isotherm of arsenite and arsenate on NL is best described by a Langmuir equation [23,24]. The Langmuir isotherm is described as

$$Y_e = \frac{Y_s C_e}{1 + k_0 C_e} \tag{1}$$

The mass transfer rate from external liquid phase to the adsorbent surface can be written as

$$N(t) = 4\pi R^2 K_f (C_t - C_{et}) \tag{2}$$

The diffusion rate of solute through the pore as per Fick's law can be expressed as

$$N(t) = \frac{4\pi D_e C_{et}}{(1/R_f) - (1/R)} \tag{3}$$

where $D_e$ is the effective diffusivity in the porous adsorbent [36]. The mass balance on a spherical element of adsorbate particle can be written as

$$N(t) = -4\pi R_f^2 Y_{et} \rho \frac{dR_f}{dt} \tag{4}$$

The mean concentration of adsorbate on adsorbent particle at any time can be written as

$$\bar{Y}_t = Y_{et}\left[1 - \left(\frac{R_f}{R}\right)^3\right] \tag{5}$$

The differential mass balance over the system is obtained by equating the decrease in adsorbate concentration in the solution with the accumulation of adsorbate in the adsorbent

$$N(t) = -V\frac{dC_t}{dt} = W\frac{d\bar{Y}_t}{dt} \tag{6}$$

The dimensionless terms used for simplification are as follows:

$$C_t^* = \frac{C_t}{C_0}, \quad r = \frac{R_f}{R}, \quad Bi = \frac{K_f R}{D_e}, \quad Ch = \frac{W}{VC_0}, \quad C_{et}^* = \frac{C_{et}}{C_0} \quad \text{and} \quad \tau = \frac{D_e t}{R^2}$$

By combining Eqs. (1)–(6), two first order differential equations (Eqs. (7) and (8)) are obtained. The detailed mathematics involved to obtain the governing differential equations are described elsewhere [35].

$$\frac{dr}{d\tau} = f_1(C_t^*, r) \tag{7}$$

$$\frac{dC_t^*}{d\tau} = \frac{N_1(C_t^*, r) f_1(C_t^*, r)}{M(C_t^*, r)} = f_2(C_t^*, r) \tag{8}$$

where

$$f_1 = \frac{-Bi\,(C_0/\rho Y_{et})\,(C_t^* - C_{et}^*)}{r^2} \tag{9}$$

$$M = 1 + Ch(1 - r^3)\frac{Y_{es} Bi(1 - r)}{(1 + k_0^* C_{et}^*)^2\,[r + (1 - r)Bi]} \tag{10}$$

$$N_1 = 3\,Ch Y_{et} r^2 + \frac{Ch\,Y_{es}\,Bi(1 - r^3)C_t^*}{(1 + k_0^* C_{et}^*)^2 [r + (1 - r)Bi]^2} \tag{11}$$

$$Y_{es} = Y_s C_0 \quad \text{and} \quad k_0^* = k_0 C_0$$

The initial conditions for these equations are $C_t^* = 1.0$ and $r = 1.0$ at $\tau = 0.0$. Eqs. (7) and (8) can be solved simultaneously to find the bulk concentration–time curve if all the process parameters ($K_f$ and $D_e$) are known. These two parameters are estimated by comparing the calculated concentration profile with the experimental data as outlined in the next section.

## 3. Numerical method

Eqs. (7) and (8) are solved using fourth order Runge-kutta method with a step size ($d\tau$) of the order $10^{-5}$ with a guess values of the parameters ($D_e$ and $K_f$), to compute the bulk concentration profile of arsenic species. At every time point of measurements, the calculated and experimental values of the concentration are compared and sum of square errors (SSE) function is calculated using Eq. (12):

$$\text{SSE} = \sum_{i=1}^{n} \{C^*_{t,\text{exp}} - C^*_{t,}\}_i^2 \tag{12}$$

The final sets of the parameters are obtained by minimizing SSE function. For this purpose, optimization subroutine UNLSF/DUNLSF from IMSL math library has been used that employs a direct search algorithm.

## 4. Experimental materials and methods

### 4.1. Preparation of As(V) and As(III) stock solutions

As(V) and As(III) stock solutions (1000 mg/l) were prepared by dissolving sodium arsenate ($NaH_2AsO_4{\cdot}7H_2O$, Merck, Germany) and sodium arsenite ($NaAsO_2$, Merck, Germany) in double distilled water, respectively. Working solution for experiments was freshly prepared from the stock solution. All reagents were of analytical grade and used without further purification.

### 4.2. Adsorbent

NL was collected from Midnapore district of West Bengal, India. NL was crushed by jaw crusher, washed several times by tap water until loosely bound particles were removed. After air-drying, the particles were screened to obtained within desired size range.

### 4.3. Kinetic study

Kinetic study was carried out in an agitated baffled vessel (internal diameter, 0.095 m; height, 0.17 m; number of baffles, 4; baffle clearance, 0.05 m; capacity, 0.7 l) made of stainless steel (SS-316). The vessel was kept in a constant temperature bath and equipped with a three-blade impeller (diameter, 0.04 m). The data, simulated in this study are obtained from the kinetic study performed in the earlier studies using above said experimental setup [23,24]. In this study, the kinetic data obtained for various operating parameters analyzed by the model were stirrer rpm: 1200–2600, initial As(V) concentration: 1–5 mg/l; initial As(III) concentration: 1–3 mg/l; varying particle size: 0.25–0.65 mm mean diameter; adsorbent dose: 10–40 g/l; temperature: 283–315 K. Two arsenic contaminated groundwater samples were collected from Dhabdhobi, Malikpur, 24 Parganas (South), West Bengal, India. Collected contaminated groundwater samples were used to perform arsenic adsorption isotherm and kinetic studies on NL at 305 K. The corresponding kinetic data were fitted to the applied model. In the later parts of the discussion, two arsenic contaminated samples were assigned as sample 1 and sample 2, respectively.

### 4.4. Analysis

The pH dependent surface charge of NL was determined by potentiometric acid–base titration method. $N_2$ gas adsorption–desorption isotherms of NL were obtained at liquid nitrogen temperature using a Quantachrom equipment (Autosorb-I). Multipoint BET surface area was obtained from the first part of isotherm ($P/P_0 < 0.3$). The chemical composition as metal oxides was measured by X-ray energy dispersive spectrometer (SEM–EDX, model: ESM-5800, GEOL, Japan). Arsenic concentration was analyzed using furnace mode of atomic absorption spectrophotometer (model: Aanalyst 700, PerkinElmer, USA) according to the method of U.S. Environmental Protection Agency (Method No.: 200.9) at a wavelength of 193.7 nm using electrodeless discharge lamp. Detection limit of this method by this instrument was 2.0 μg/l. The pH measurements were done by a pH meter (model: ZPH1-9100, ZICO, India).

**Table 1**
Characteristics of natural laterite (NL).

| Properties | Natural laterite |
|---|---|
| Particle size (spherical) (mm) | 0.3–0.5 |
| Surface area ($m^2$/g) | 17.5–18.3 |
| Pore volume (ml/g) | 0.020–0.022 |
| Bulk density (g/ml) | 1.29–1.36 |
| True density (g/ml) | 2.34–2.46 |
| $pH_{ZPC}$ | 7.4–7.5 |
| Conductivity (1:5, laterite:water mixture) (μS/cm) | 17.6–22.4 |
| pH (1:5, laterite:water mixture) | 6.65–6.86 |
| Inorganic composition (as metal oxide: wt%) | |
| Fe-oxide | 43.9–47.3 |
| $SiO_2$ | 26.5–28.5 |
| Al-oxide | 19.3–21.5 |
| $MnO_2$ | ~0.7 |
| $Na_2O$ | ~0.8 |

## 5. Results and discussion

### 5.1. Characterization of NL

The used NL as arsenic adsorbent for this study as the same material (single collection of NL sample) as it was used in our earlier studies [23,24]. The detailed chemical and physical characterization of NL is already discussed in the above said citations. Here, brief characterizations of NL with its chemical composition are presented in Table 1.

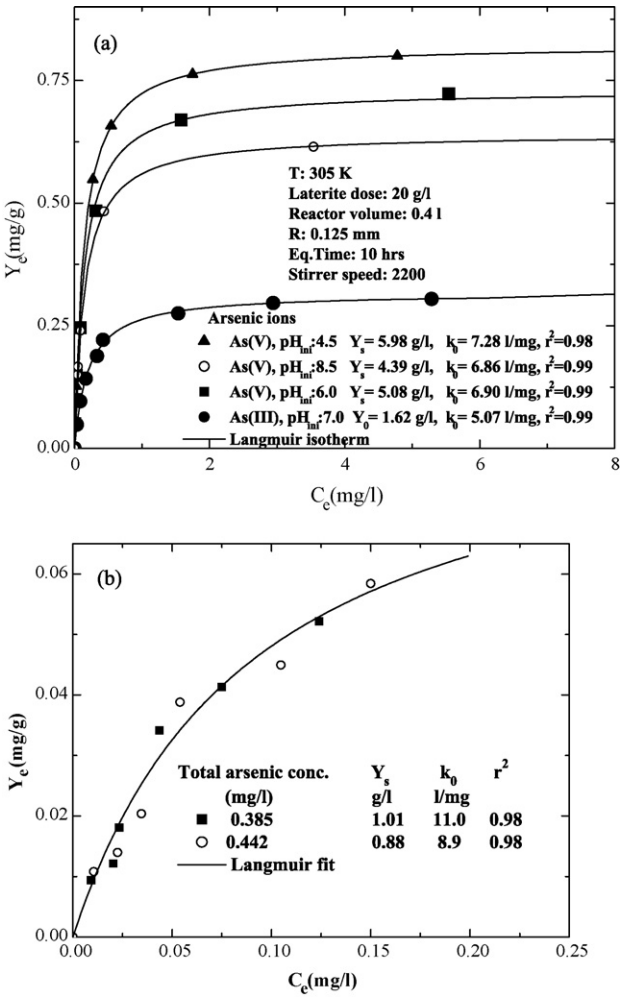


**Fig. 1.** Adsorption isotherm of (a) synthetic arsenite and arsenate solution onto NL and (b) real arsenic contaminated groundwater onto NL.

### 5.2. Langmuir isotherm parameters

The equilibrium (equilibrium time: 12 h) arsenic concentrations in the stirred tank adsorber for different initial concentrations of arsenate and arsenite at constant temperature are used to generate adsorption isotherm. The isotherm data of arsenite and arsenate on NL at 305 K are reported in Fig. 1. Fig. 1 shows that experimental isotherm data satisfactorily follow Langmuir isotherm model. Arsenate adsorption on NL surface is pH dependent [24]. Therefore, isotherm at 305 K temperature of arsenate is generated at different initial pHs of 4.5, 6.0 and 8.5. On the other hand, arsenite adsorption on NL is almost unaffected over the entire pH range of 4.5–9.0 [23]. Hence, Langmuir isotherm constants for arsenite are evaluated only at pH 7.0. The isotherm constants of arsenic species are presented in Fig. 1a. The isotherm for groundwater–NL system is presented in Fig. 1b. The corresponding constant values of the isotherm are also presented in that figure.

### 5.3. Estimated values of $D_e$ and $K_f$

It is observed that the effective pore diffusivity turns out to be almost same for both arsenite and arsenate species. This value varies in a narrow range from 2.2 to $2.6 \times 10^{-11}$ m$^2$/s at 305 K and for various particle sizes (0.25–0.65 mm). The pore diffusivity increases with temperature. For example, its value is $1.2 \times 10^{-11}$ m$^2$/s at 283 K and $5.9 \times 10^{-11}$ m$^2$/s at 315 K. It is interesting to note that the value of pore diffusivity obtained in this study is two order of magnitude less than that in the bulk liquid ($1 \times 10^{-9}$ m$^2$/s) [17], due to tortuous pathway of diffusion and pore constriction. Lin and Wu [17] obtained $D_e$ values for arsenite and arsenate species onto activated alumina (AA) particles in the range $1 \times 10^{-11}$ to $5 \times 10^{-12}$ m$^2$/s. In the present study, it is observed that the optimized $D_e$ values are independent of initial arsenic concentration, stirrer speed and dose of adsorbent.

The estimated values of external mass transfer coefficient ($K_f$) are found to be a function of stirrer speed only. It increases from $0.13 \times 10^{-6}$ to $1.4 \times 10^{-6}$ m/s with increase in stirrer speed from 1200 to 2600 rpm. The sum of square errors (SSE) between the calculated and experimental concentration data is evaluated for each set of kinetic run and values are reported in the corresponding figures.

### 5.4. Parametric study

Various parameters that affect the adsorption kinetics are—the initial adsorbate concentration in liquid, the ratio of the mass of

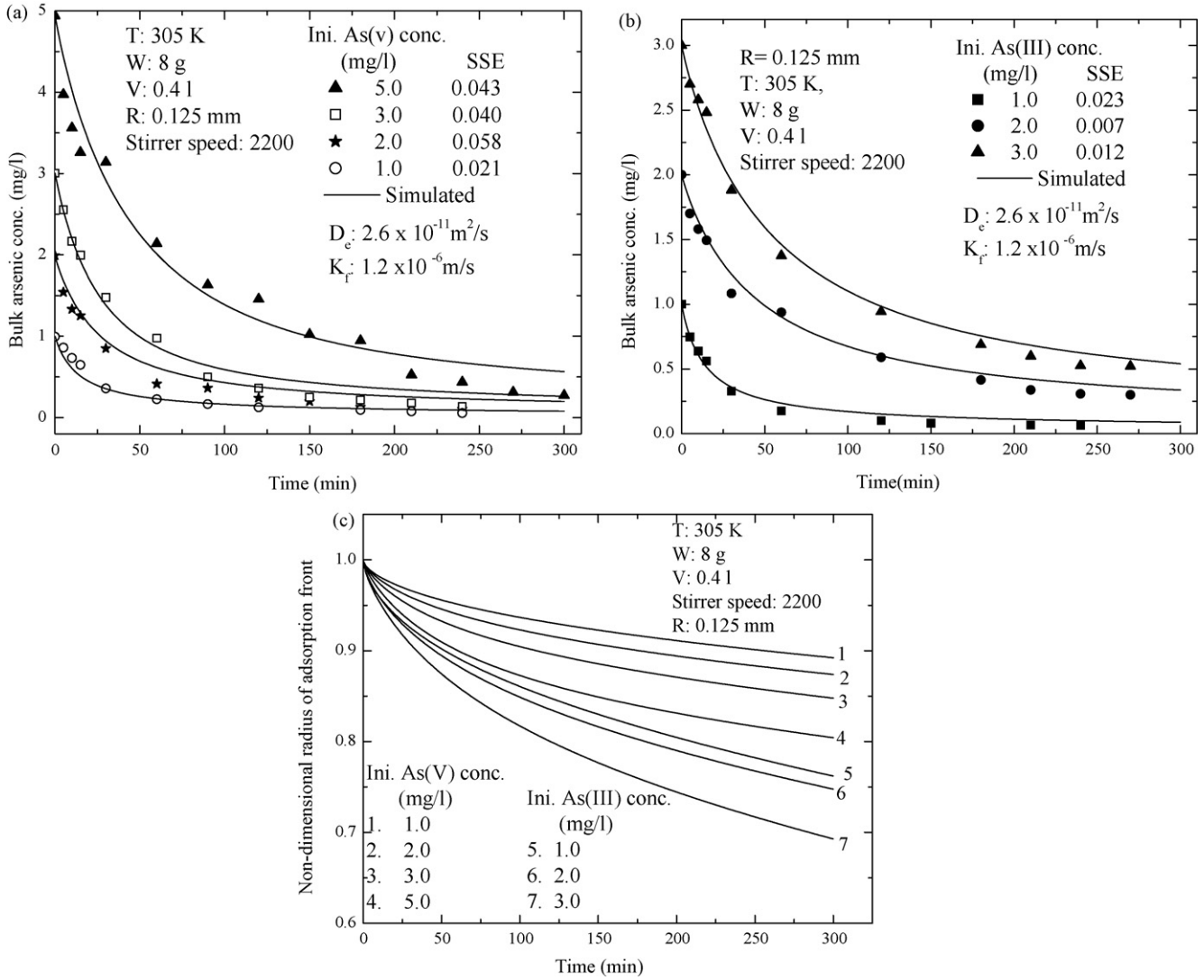


**Fig. 2.** (a) Bulk concentration–time curve in the stirrer tank adsorber for different initial As(V) concentrations. (b) Bulk concentration–time curve in the stirrer tank adsorber for different initial As(III) concentrations. (c) Simulated non-dimensional radius of adsorption front for different initial As(V) and As(III) concentrations.

adsorbent to the solution volume, stirrer speed, the particle size of adsorbent, temperature, others ions present in the solution, etc.

*5.4.1. Effect of initial adsorbate concentration*

The effects of the initial adsorbate concentration on the bulk concentration decay profiles of both arsenite and arsenate ions are presented in Fig. 2a and b, respectively. From these figures, it is clear that, the simulated bulk concentration–time curves of both adsorbate ions initially (~150 min) follow the experimental decay curve closely. In the later part of adsorption, some deviations are observed. The trend of deviation for each experimental set of data with simulated profile is similar, i.e., the simulated value of bulk concentration is always found to be more than the experimental data in the later part of the experiments (beyond 150 min). This observation may be explained as follows. In prolonged operation, some NL particles break under high stirring speed (2200 rpm), leading to generation of more active surface area. On the other hand, in this model, the particle diameter is taken as constant to its initial average value. Thus, model calculations show lower extent of adsorption compared to the experimental observation.

The simulated dimensionless radius ($r$) of adsorption front as a function of time for various arsenate and arsenite concentrations is presented in Fig. 2c. The unadsorbed core is decreasing at a faster rate for higher initial adsorbate concentration due to higher availability of adsorbate ions. For example, in Fig. 2c, the slope of the curves 1, 2 and 3 decreases in that order. With increase in initial adsorbate ion concentration, the reaction front shrinks at a higher rate. The adsorption capacity of NL towards arsenate species is higher compared to arsenite species. Thus, unadsorbed core decreases faster for arsenite at the same initial concentration and under identical experimental conditions. For example, with 3.0 mg/l initial arsenite (curve 7 in Fig. 2c) and arsenate (curve 3 in Fig. 2c) concentration, the adsorption front travels almost 30% and 15%, respectively, over a period of about 300 min.

*5.4.2. Effect of temperature*

The decay of bulk concentration of both arsenite and arsenate is faster at higher temperature (figure not shown here). This is due to increase in mobility of adsorbate species, which leads to higher rate of adsorption of arsenic species onto NL at higher temperature. The values of $D_e$ increase from $1.2 \times 10^{-11}$ m$^2$/s at 283 K to $5.9 \times 10^{-11}$ m$^2$/s at 315 K temperature for ~5.0 mg/l initial arsenate concentration.

*5.4.3. Effect of particle size*

The effect of particle size on decay of bulk concentration of arsenate ion is presented in Fig. 3. The rate of decay of bulk concentration is faster for lower particle diameters, which is due to availability of higher surface area in the smaller sized particles.

*5.4.4. Effect of Biot number*

The Biot number (Bi) of the system is defined as $Bi = K_f R/D_e$. Biot number is an important parameter to quantify the film diffusion contribution in the total mass transfer mechanism. Biot number represents the ratio of the rate of transport across the liquid layer to the rate of diffusion into the pore of the particle. For $Bi \ll 1$, the adsorption rate is external mass transfer resistance controlled. While for $Bi \gg 100$, pore diffusion is the predominant mass transfer controlling mechanism [37]. From computed values of $K_f$ corresponding to various stirrer speeds, it is observed that Biot number in this study varies from 0.75 to 9.0 (please see Fig. 4). Therefore, both external mass transfer resistance and pore diffusion are important in this adsorption process. The effect of Biot number on the profile of bulk concentration is presented in Fig. 4. It is clearly observed from Fig. 4 that the decay rate increases with increase in Biot number.

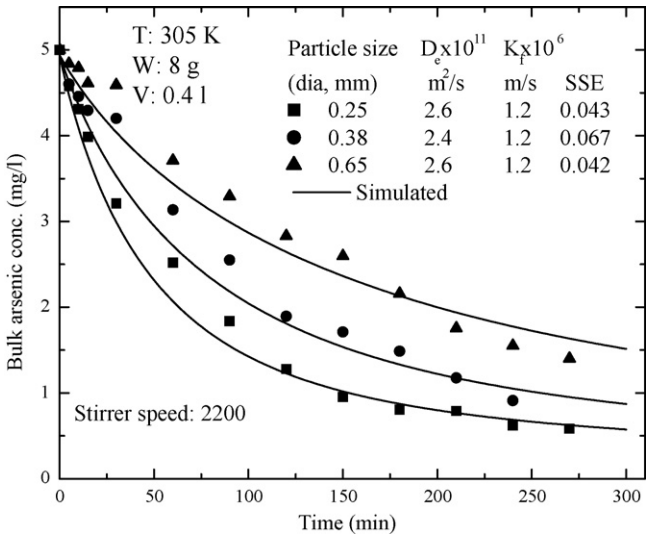


**Fig. 3.** Adsorbent particle size effect on bulk concentration–time curve for fixed As(V) ions concentration.

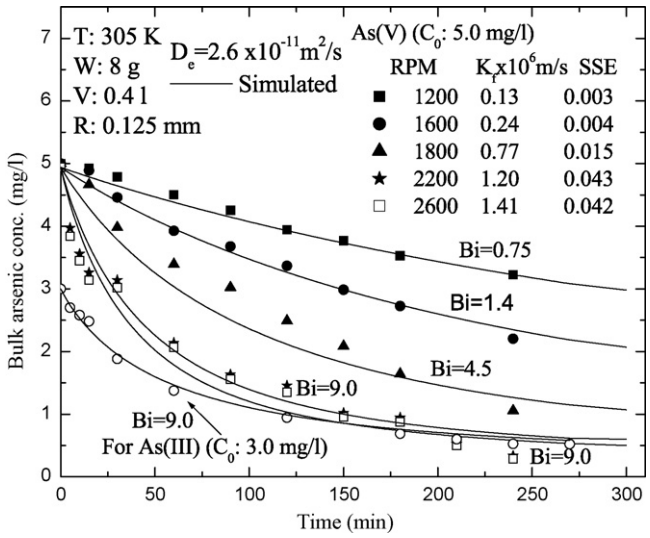


**Fig. 4.** Bulk concentration–time curve for different stirrer rpms at a fixed arsenic concentration.

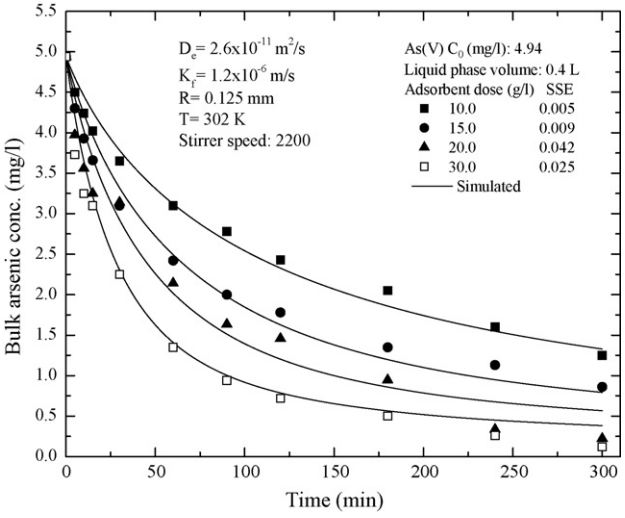


**Fig. 5.** Effect of adsorbent dose on bulk concentration–time curve for fixed initial As(V) ions concentration.

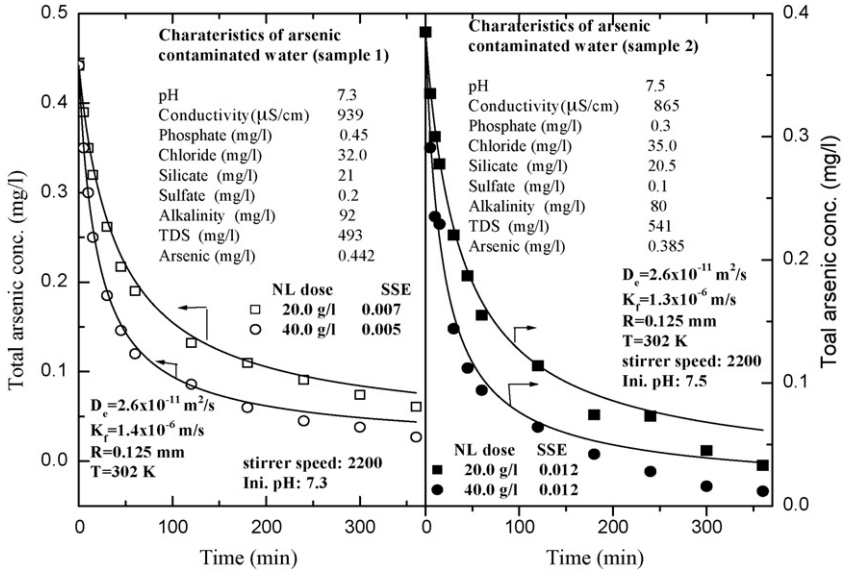


**Fig. 6.** Arsenic adsorption kinetics of arsenic contaminated groundwater on NL.

At higher Biot number (i.e., at higher $K_f$) the thickness of external mass transfer film is less due to higher turbulence. This tends to higher transport of adsorbate species to the active sites of adsorbent resulting into higher rate of adsorption.

*5.4.5. Effect of the mass of adsorbent to the solution volume*

The adsorbent mass is varied with a constant reaction volume. Fig. 5 shows the effect of NL dose on bulk concentration decay of arsenate species for fixed volume of solution (0.4 l). With the increase in mass of adsorbent at constant reaction volume, the concentration decay of adsorbate species is sharper. This is due to fact that with an increase in adsorbent amount, the adsorption sites increase, so rapid decrease in liquid phase concentration is observed.

*5.4.6. Arsenic adsorption kinetics of arsenic contaminated groundwater on NL*

The experimental results in Fig. 2a and b indicate that arsenite removal is slower from solution compared to arsenate. As per finding of this model, it is observed that parameters $D_e$ and $K_f$ are found to be independent of the nature of the arsenic species, the difference in the rates of uptake is due to the differences in the adsorption isotherm constants only. Therefore, the present model is easily applied to any arsenic contaminated water and NL system. Two different samples of contaminated water have been collected from two tube well in the affected area. Adsorption study of real contaminated water samples has been undertaken using NL. Characterizations of these water samples are presented in Fig. 6. To apply the present model to this real system, first Langmuir isotherm constants are evaluated. These are presented in Fig. 1b. $D_e$ and $K_f$ values corresponding to synthetic solution have been used to predict the concentration decay curve of arsenic using this model. The sum of square errors (SSE) between predicted and experimental data is calculated and the low values (0.005–0.012) of SSE indicate satisfactory performance of applied model to real arsenic contaminated groundwater–NL system.

## 6. Conclusion

(i) The effective pore diffusivity ($D_e$) obtained is almost in the same range for both arsenite and arsenate species on natural laterite. This value varies in the narrow range from 2.2 to $2.6 \times 10^{-11}$ m$^2$/s at 305 K and for various particle sizes (0.2–0.65 mm).

(ii) It is observed that the optimized $D_e$ values are independent of initial concentration of arsenic, pH of solution, stirrer speed and dose of adsorbent, but dependent on temperature and particle size of adsorbent.

(iii) The external mass transfer coefficient ($K_f$) is independent of arsenic species, concentration of arsenic, pH of solution, particle size and dose of adsorbent. But it varies strongly with stirrer speed. It increases from $1.0 \times 10^{-6}$ to $1.4 \times 10^{-6}$ m/s with increase in stirrer speed from 1200 to 2600 rpm.

(iv) The arsenate and arsenite adsorption on NL is controlled by both external film resistance and pore diffusion mass transfer phenomenon.

(v) The present model results satisfactory prediction for concentration decay of total arsenic in real contaminated groundwater and NL system during batch adsorption.

## Acknowledgements

This work is partially supported by a grant from the Department of Science and Technology, New Delhi, Government of India under the scheme no. DST/TDT/WTI/2K7/04, New Delhi, Government of India. Any opinions, findings and conclusions expressed in this paper are those of the authors and do not necessarily reflect the views of DST.

## References

[1] S.K. Acharyya, S. Lahiri, B.C. Raymahashay, A. Bhowmik, Arsenic toxicity of groundwater in parts of the Bengal basin in India and Bangladesh: the role of quaternary stratigraphy and Holocene sea-level fluctuation, Environ. Geol. 39 (2000) 1127–1137.
[2] C.F. Harvey, C.H. Swartz, A.B.M. Badruzzaman, N. Keon-Blute, W. Yu, M.A. Ali, J. Jay, R. Beckie, V. Niedan, D. Brabander, P.M. Oates, K.N. Ashfaque, S. Islam, H.F. Hemond, M.F. Ahmed, Arsenic mobility and groundwater extraction in Bangladesh, Science 298 (2002) 1602–1606.
[3] A.H. Welch, M.S. Lico, J.L. Hughes, Arsenic in ground water of the Western United States, Ground Water 26 (1988) 333–347.
[4] J.M. Borgoño, P. Vincent, H. Venturino, A. Infante, Arsenic level in river water supply of Antafagosa Chile, Environ. Health Perspect. 19 (1977) 103–105.
[5] L.M. Del Razo, M.A. Arellano, M.E. Cebarian, The oxidation states of arsenic in well-water from a chronic arsenicism area of northern Mexico, Environ. Pollut. 64 (1990) 143–153.

[6] S.-L. Chen, S.R. Dzeng, M.-H. Yang, K.-H. Chiu, G.-M. Shieh, C.M. Wai, Arsenic species in groundwaters of the blackfoot disease area, Taiwan, Environ. Sci. Technol. 28 (1994) 877–881.
[7] I.A. Katsoyiannis, A.I. Zouboulis, M. Jekel, Kinetics of bacterial As(III) oxidation and subsequent As(V) removal by sorption onto biogenic manganese oxides during groundwater treatment, Ind. Eng. Chem. Res. 43 (2004) 486–493.
[8] H.K. Hansen, P. Núñez, R. Grandon, Electrocoagulation as a remediation tool for wastewaters containing arsenic, Miner. Eng. 19 (2006) 521–524.
[9] S.R. Wickramasinghe, B. Han, J. Zimbron, Z. Shen, M.N. Karim, Arsenic removal by coagulation and filtration: comparison of groundwaters from the United States and Bangladesh, Desalination 169 (2004) 231–244.
[10] M. Hodi, K. Polyak, J. Hlavay, Removal of pollutants from drinking water by combined ion exchange and adsorption methods, Environ. Int. 21 (1995) 325–331.
[11] K. Košutić, L. Furač, L. Sipos, B. Kunst, Removal of arsenic and pesticides from drinking water by nanofiltration membranes, Sep. Purif. Technol. 42 (2005) 137–144.
[12] T. Urase, J.-I. Oh, K. Yamamoto, Effect of pH on rejection of different species of arsenic by nanofiltration, Desalination 117 (1998) 11–18.
[13] D. Mohan C.U.Jr., Pittman, Arsenic removal from water/wastewater using adsorbent—a critical review, J. Hazard. Mater. 142 (2007) 1–53.
[14] T.S.Y. Choong, T.G. Chuah, Y. Robiah, F.L.G. Koay, I. Azni, Arsenic toxicity, health hazards and removal techniques from water: an overview, Desalination 217 (2007) 139–166.
[15] T.S. Singh, K.K. Pant, Equilibrium, kinetics and thermodynamic studies for adsorption of As(III) on activated alumina, Sep. Purif. Technol. 36 (2004) 139–147.
[16] T.S. Singh, K.K. Pant, Experimental and modeling studies on fixed bed adsorption of As(III) ions from aqueous solution, Sep. Purif. Technol. 42 (2005) 265–296.
[17] T.-F. Lin, J.-K. Wu, Adsorption of arsenite and arsenate within activated alumina grains: equilibrium and kinetics, Water Res. 35 (2001) 2049–2057.
[18] M. Jang, W. Chen, F.S. Cannon, Preloading hydrous ferric oxide into granular activated carbon for arsenic removal, Environ. Sci. Technol. 42 (2008) 3369–3374.
[19] S. Dixit, J.G. Hering, Comparison of arsenic (V) and arsenic (III) sorption onto iron oxide minerals: implications for arsenic mobility, Environ. Sci. Technol. 37 (2003) 4182–4189.
[20] B.A. Manning, M.L. Hunt, C. Amrhein, J.A. Yarmoff, Arsenic(III) and arsenic (V) reactions with zerovalent iron corrosion products, Environ. Sci. Technol. 36 (2002) 5455–5461.
[21] B.A. Manning, S.E. Fendrof, B. Bostick, D.L. Suarez, Arsenic(III) oxidation and arsenic (V) adsorption reactions on synthesis birnessite, Environ. Sci. Technol. 36 (2002) 976–981.
[22] P. Lakshmipatthiraj, B.R.V. Narashimhan, S. Prabhakar, G. Bhaskarraju, Adsorption of arsenate on synthetic goethite from aqueous solutions, J. Hazard. Mater. 136 (2006) 281–287.
[23] A. Maiti, S. Dasgupta, J.K. Basu, S. De, Adsorption of arsenite using natural laterite as adsorbent, Sep. Purif. Technol. 55 (2007) 350–359.
[24] A. Maiti, S. Dasgupta, J.K. Basu, S. De, Batch and column study: adsorption of arsenate using untreated laterite as adsorbent, Ind. Eng. Chem. Res. 47 (2008) 1620–1629.
[25] S.K. Maji, A. Pal, T. Pal, Arsenic removal from real-life groundwater by adsorption on laterite soil, J. Hazard. Mater. 151 (2008) 811–820.
[26] F. Partey, D. Norman, S. Ndur, R. Nartey, Arsenic sorption onto laterite iron concretions: temperature effect, J. Colloid Interface Sci. 321 (2008) 493–500.
[27] L. Cumbal, A.K. Sengupta, Arsenic removal using polymer-supported hydrated iron (III) oxide nanoparticles: roles of Donnan membrane effect, Environ. Sci. Technol. 39 (2005) 6508–6515.
[28] Y. Lee, I.-H. Um, J. Yoon, Arsenic (III) oxidation by Iron (IV) (ferrate) and subsequent removal of arsenic (V) by iron (III) coagulation, Environ. Sci. Technol. 37 (2003) 5750–5756.
[29] M.A. Lopez-Anton, M. Diaz-Somoano, D.A. Spears, M.R. Martinez-Tarazona, Arsenic and selenium capture by fly ashes at low temperature, Environ. Sci. Technol. 40 (2006) 3947–3951.
[30] K.P. Raven, A. Jain, R.H. Loeppert, Arsenite and arsenate adsorption on ferrihydrite: kinetics, equilibrium, and adsorption envelopes, Environ. Sci. Technol. 32 (1998) 344–349.
[31] P. Chutia, S. Kato, T. Kojima, S. Satokawa, Arsenic adsorption from aqueous solution on synthetic zeolites, J. Hazard. Mater. 162 (2009) 440–447.
[32] X.-H. Guan, T. Su, J. Wang, Quantifying effects of pH and surface loading on arsenic adsorption on nano active alumina using a speciation-based model, J. Hazard. Mater. 166 (2009) 39–45.
[33] G. Muñiz, V. Fierro, A. Celzard, G. Furdin, G. Gonzalez-Sánchez, M.L. Ballinas, Synthesis, characterization and performance in arsenic removal of iron-doped activated carbons prepared by impregnation with Fe(III) and Fe(II), J. Hazard. Mater. 165 (2009) 893–902.
[34] D. Ranjan, M. Talat, S.H. Hasan, Biosorption of arsenic from aqueous solution using agricultural residue 'rice polish', J. Hazard. Mater. 166 (2009) 1050–1059.
[35] P.R. Jena, S. De, J.K. Basu, A generalized shrinking core model applied to batch adsorption, J. Chem. Eng. 95 (2003) 143–154.
[36] H.S. Fogler, Elementals of Chemical Reaction Engineering, 2nd ed., Prentice-Hall, New Delhi, India, 1997.
[37] K.K.H. Choy, J.F. Porter, G. Mckay, Film-pore diffusion models—analytical and numerical solutions, Chem. Eng. Sci. 59 (2004) 501–512.